1987

A Mathematical Model of a Zinc/Bromine Flow Cell

T. I. Evans
Texas A & M University - College Station

Ralph E. White
University of South Carolina - Columbia, white@cec.sc.edu

Publication Info

Journal of the Electrochemical Society, 1987, pages 866-874.

http://www.electrochem.org/
DOI: 10.1149/1.2100588
http://dx.doi.org/10.1149/1.2100588

U superficial velocity, cm s^{-1}
V volume, cm^3
ΔV volume of bed element, cm^3
w bed width, cm
X concentration of benzoquinone in organic phase, m.f.
$\bar{y}$ dependent variable — predicted value
y dependent variable — measured value
z number of electrons

Greek

α electrochemical charge transfer coefficient
β liquid holdup
γ $K_S(1 - K_S/(K_L + K_S))$
δ $K_L K_S[B]_e(1 - X)/(K_L + K_S)$
ϵ bed voidage
η overpotential, V
θ parameter value-posterior estimate
θ^* parameter value-prior estimate
κ_S conductivity of anode bed, mho cm^{-1}
κ_L conductivity of electrolyte solution, mho cm^{-1}
κ_f conductivity of feeder electrode, mho cm^{-1}
μ viscosity, g cm s^{-1}
ρ density, g cm^{-3}
σ standard deviation
ϕ potential, V
Φ objective function
ψ $Sk_2 \exp(\alpha_2 \phi \mathbf{F}/RT)\ 6\mathbf{F}$

Subscripts

aq in aqueous phase
org in organic phase
e equilibrium value
L liquid phase
G gas phase
S solid phase
i reaction number
j thickness increment number
k length increment number
m dependent variable number
n parameter number

REFERENCES

1. R. Alkire, *AIChE Symp. Ser.* No. 204, **77,** 121 (1981).
2. R. Alkire and P. Ng, *This Journal,* **124,** 1220 (1977).
3. R. Alkire and R. Gould, *ibid.,* **127,** 605 (1979).
4. R. Alkire and S. Soon, and M. Stadtherr, *ibid.,* **132,** 1105 (1985).
5. M. Paulin, D. Hutin, and F. Coeuret, *ibid.,* **124,** 180 (1977).
6. G. Kreysa, *Electrochim. Acta,* **23,** 1351 (1978).
7. G. Skellaropoulos and G. Francis, *This Journal,* **126,** 1928 (1979).
8. A. W. Bryson and K. A. Dardis, *J. Chem. Tech. Biotech.,* **30,** 14 (1980).
9. F. Goodridge and M. A. Hamilton, *Electrochim. Acta,* **25,** 481 (1980).
10. M. Fleischmann and R. Jansson, *ibid.,* **27,** 1029 (1982).
11. J. Lee, *AIChE Symp. Ser.* No. 229, **79,** 111 (1983).
12. J. Van Zee and R. White, *This Journal,* **132,** 818 (1985).
13. C. Oloman, *J. App. Electrochem.,* **10,** 553 (1980).
14. J. G. Schwartz, E. Wager, and M. P. Dudukovic, *AIChE J.,* **22**(5), 953 (1976).
15. M. Herskowitz and J. M. Smith, *ibid.,* **29,** 1 (1983).
16. J. S. Clarke, R. E. Ehigamusee, and A. T. Kuhn, *J. Electronal. Chem. Interfacial Electrochem.,* **70,** 333 (1976).
17. S. Ito, K. Sasaki, Y. Murakami, and H. Shiba, *Denki Kagaku,* **40**(10), 733 (1972).
18. A. T. Kuhn, *Chem. Ind.,* 867 (Oct. 16, 1976).
19. R. Von Wetzel, L. Muller, and P. Gottlieb, *Z. Phys. Chem.,* **258**(3), 528 (1977).
20. C. Oloman, *This Journal,* **126,** 1885 (1979).
21. L. A. Leacock and S. W. Churchill, *AIChE J.,* **7,** 196 (1961).
22. P. Lu and R. Alkire, *This Journal,* **131,** 1059 (1984).
23. K. Takahashi and R. Alkire, *Chem. Eng. Commun.,* **38,** 209 (1985).
24. G. Box, P. Box, and G. C. Tiao, "Bayesian Inference in Statistical Analysis," Addison-Wesley Publishing Co., Reading, MA (1973).
25. T. W. Hoffman and P. M. Reilly, *Can. J. Chem. E.,* **57,** 367 (1979).
26. P. M. Reilly and H. Patino-Leal, *Technometrics,* **23,** 221 (1981).
27. "Chemical Engineers' Handbook," 5th ed., R. H. Perry and C. H. Chiltern, Editors, McGraw Hill, Inc., New York (1973).
28. "Chemical Engineers' Handbook," 3rd ed., p. 1783, J. H. Perry, Editor, McGraw-Hill, Inc., New York (1950).
29. H. Cerfontain, *Rec. Trav. Chim.,* **84,** 491 (1965).
30. D. J. Pickett, "Electrochemical Reactor Design," p. 71, Elsevier Publishing Co., New York (1977).
31. "Handbook of Chemistry and Physics," 56th ed., R. C. Weast, Editor, p. D172, CRC Press (1976).

A Mathematical Model of a Zinc/Bromine Flow Cell

T. I. Evans* and R. E. White**

Department of Chemical Engineering, Texas A&M University, College Station, Texas 77843

ABSTRACT

A mathematical model is presented for a zinc/bromine flow cell. The model includes a thin porous layer on the bromine electrode and a porous separator. The independent parameters of the porous layer are defined, and their effect on cell performance during charge and discharge is investigated. The dependence of the round trip energy efficiency on the thickness of the porous layer and mode of discharge is presented. The predictions of the model show that a maximum round trip energy efficiency of 70% should be possible under the design conditions considered.

The zinc/bromine (Zn/Br_2) flow battery has received considerable interest in recent years as a durable, rechargeable storage battery for applications such as vehicle propulsion and leveling of peak electricity usage. Several companies are developing this battery by building and testing various designs (1). A mathematical model of a single cell of one of these designs is presented, and it is hoped that the model will reduce the costs associated with developing the Zn/Br_2 battery.

The model is an extension of that presented by Mader and White (2) and can be used to predict the round trip energy efficiency of the cell. The extensions include a porous layer on the bromine electrode and the ability to predict the performance of the cell during discharge. Predictions for both charge and discharge modes can be made for both constant cell potential and constant current conditions.

Other models (3-6) of the Zn/Br_2 flow cell have been presented but are of limited utility for one reason or another. For example, Lee and Selman (3, 4) presented models of the Zn/Br_2 cell which were developed primarily to study the effect of terminal tab location on the current distribution along the electrodes and to study the growth of dendrites due to the uneven plating of zinc. Consequently, their model cannot be used to account for a porous layer on the bromine electrode nor predict round trip energy efficiencies. Van Zee *et al.* (5) presented a simple Zn/Br_2 battery model, but their model does not have the capability of predicting product con-

*Electrochemical Society Student Member.
**Electrochemical Society Active Member.

versions, which is a necessary feature to follow the state-of-charge of the cell. Fedkiw and Watts (6) developed a comprehensive mathematical model for the iron/chromium (Fe/Cr) redox cell (7) which is similar to some Zn/Br_2 cell designs (1) but not the one presented here.

Model Development

The model presented here is an extension of the model of a single Zn/Br_2 flow cell on charge published earlier by Mader and White (2). This extension includes using a thin porous electrode as the bromine electrode, as shown schematically in Fig. 1. The assumptions and equations used by Mader and White (2) are the same as before. The additional assumptions and descriptive equations for the porous electrode are presented next.

Assumptions.—The following additional assumptions were made in the development of the equations for the porous electrode region of the model. It is assumed that species can only diffuse and migrate into and out of the porous region (*i.e.*, no convective transport exists within the porous electrode). This assumption seems reasonable as long as the thickness of the porous electrode (S_{PE}) is much less than the channel gap (S_A). Next, it is assumed that the homogeneous complexation reaction producing tribromide occurring in the electrolyte bulk also occurs in the electrolyte contained within the pores of the porous electrode and is in equilibrium throughout, as it is in the bulk. Also, it is assumed that there is no potential drop in the solid phase of the porous electrode. Lastly, the electrochemical reaction within the porous region is assumed to be represented by a pseudo-homogeneous reaction rate expression based on the Butler-Volmer equation.

Governing equations.—The cell illustrated in Fig. 1 can be divided into four regions — two electrolyte flow channels of width S_A, a separator of width S_S, and a porous electrode of width S_{PE}. The governing equations for the flow channels and the separator are the electroneutrality condition, and the steady-state material balance equations for each species, as presented earlier by Mader and White (2). The equations pertaining only to the porous electrode region are the electroneutrality condition and a modified material balance equation for each species, as discussed next.

The electroneutrality condition

$$\sum_i z_i c_i = 0 \qquad [1]$$

ensures that positive and negative charges balance at every point in the electrolyte. The steady-state material balance equations for all of the species considered are

$$-\nabla \cdot \mathbf{N}_i + R_i + R'_i = 0 \qquad (i = Br^-, Br_2) \qquad [2]$$

$$-\nabla \cdot \mathbf{N}_i + R_i = 0 \qquad (i = Br_3^-) \qquad [3]$$

$$\nabla \cdot \mathbf{N}_i = 0 \qquad (i = Na^+, Zn^{2+}) \qquad [4]$$

where

$$\mathbf{N}_i = -D_{i,e,PE}\nabla c_i - z_i \frac{D_{i,e,PE}}{RT} \mathbf{F} c_i \nabla \Phi \qquad [5]$$

It should be mentioned here that Eq. [1]-[5] are presented in vector notation for convenience. The actual equations solved include gradients in the y direction only since the one-step model approach (2, 8) is used here. The R_i term in Eq. [2] and [3] represents the rate of production of species i by homogeneous reaction and R'_i in Eq. [2] represents the rate of production of species i by pseudo-homogeneous electrochemical reaction in the porous electrode, as discussed further below. The diffusion coefficient for species i in Eq. [5] is an effective diffusion coefficient and is defined here as

$$D_{i,e,PE} = \frac{D_i}{N_{m,PE}} \qquad [6]$$

where $N_{m,PE}$ is the MacMullin number for the porous electrode. This concept of a MacMullin number for the porous electrode is similar to that proposed earlier by Caldwell *et al.* (9), as discussed further by Poush *et al.* (10) and Van Zee (11), for a nonconductive porous media. The $N_{m,PE}$ concept is appealing because of its definition

$$N_{m,PE} = \frac{\tau}{\epsilon} \qquad [7]$$

where ϵ and τ are the porosity and tortuosity of the porous electrode, respectively. Unfortunately, it is unlikely that $N_{m,PE}$ can be determined directly by measuring the resistivity of the porous electrode saturated with electrolyte because of the electrochemical reactions that would occur.

Equations [2] and [3] (the three governing equations for c_{Br^-}, c_{Br_2}, and $c_{Br_3^-}$) can be simplified by recognizing that $R_{Br^-} = R_{Br_2} = -R_{Br_3^-}$ when the homogeneous complexation reaction between Br^-, Br_2, and Br_3^- is assumed to be at equilibrium. Adding Eq. [2] and [3] to eliminate R_i

$$(-\nabla \cdot \mathbf{N}_i + R_i + R'_i) + (-\nabla \cdot \mathbf{N}_{Br_3^-} + R_{Br_3^-}) = 0 \qquad (i = Br^-, Br_2) \qquad [8]$$

yields

$$\nabla \cdot \mathbf{N}_{Br^-} + \nabla \cdot \mathbf{N}_{Br_3^-} - R'_{Br^-} = 0 \qquad [9]$$

$$\nabla \cdot \mathbf{N}_{Br_2} + \nabla \cdot \mathbf{N}_{Br_3^-} - R'_{Br_2} = 0 \qquad [10]$$

The third equation needed is the equilibrium expression

$$K_{eq} = \frac{c_{Br_3^-}}{c_{Br^-} c_{Br_2}} = 17M^{-1} = 17{,}000 \text{ (mol/cm}^3\text{)}^{-1} \qquad [11]$$

where the equilibrium constant is given by Eigen and Kustin (12). Equations [1], [4], [9], [10], and [11] are the six governing equations for the six unknowns, c_i and Φ, in the porous electrode.

By converting to dimensionless variables

$$\eta = y/S \qquad [12]$$

$$\theta_i = c_i/c_{i,ref} \qquad [13]$$

the divergence of the flux of species i, $\nabla \cdot \mathbf{N}_i$, in Eq. [4], [9], and [10] can be rewritten approximately as

$$\frac{S^2 N_{m,PE}}{c_{i,ref} D_i} (\nabla \cdot \mathbf{N}_i) \approx -\frac{\partial^2 \theta_i}{\partial \eta^2} - \frac{z_i \mathbf{F}}{RT}\left[\theta_i \frac{\partial^2 \Phi}{\partial \eta^2} + \frac{\partial \theta_i}{\partial \eta}\frac{\partial \Phi}{\partial \eta}\right] \qquad [14]$$

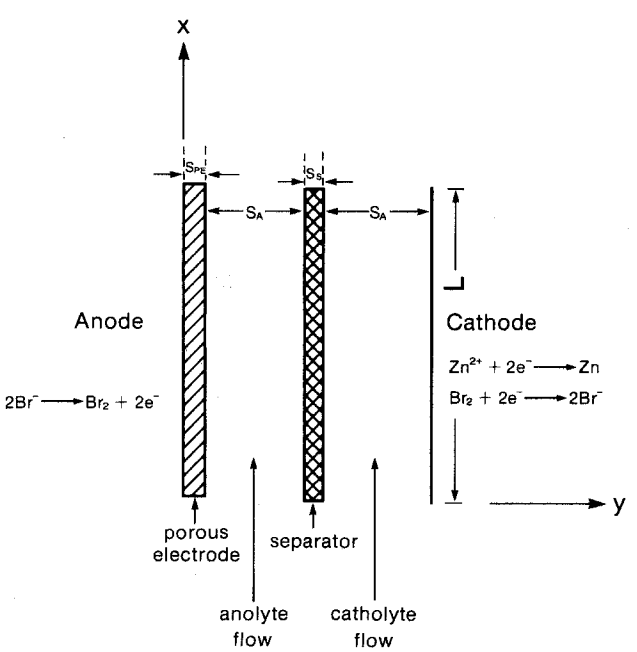

Fig. 1. Schematic of the Zn/Br_2 flow cell on charge

The gradients of θ_i and Φ in the axial (or flow) direction on the right-hand side of Eq. [14] have been omitted because when the aspect ratio ($\alpha = S/L$) is small as it is here, the diffusion and migration terms of the flux expression in the axial direction are negligible relative to the radial (or normal to flow) diffusion and migration terms as demonstrated by Nguyen *et al.* (13).

The production rate of species i due to all of the electrochemical reactions that it may be involved in within the porous electrode (R'_i) is given by

$$R'_i = -\sum_j \frac{a s_{ij} j_j}{n_j \mathbf{F}} \quad [15]$$

where a is the specific electroactive surface area of the porous material and j_j is the current density due to electrochemical reaction j based on the electroactive surface area within the porous electrode. The Butler-Volmer equation is used to determine j_j

$$j_j = i_{oj,ref}\left\{\prod_i (\theta_i)^{p_{ij}} \exp\left(\frac{\alpha_{aj}\mathbf{F}}{RT}\eta_j\right) - \prod_i (\theta_i)^{q_{ij}} \exp\left(\frac{-\alpha_{cj}\mathbf{F}}{RT}\eta_j\right)\right\} \quad [16]$$

where θ_i is the dimensionless local surface concentration and η_j is the total local overpotential which is defined as

$$\eta_j = V_{PE} - \Phi - U_{j,ref} \quad [17]$$

The open-circuit potential, $U_{j,ref}$, in Eq. [17] is given by

$$U_{j,ref} = U_j^\theta - U_{RE}^\theta - \frac{RT}{n_j\mathbf{F}}\sum_i^n s_{ij} \ln\left(\frac{c_{i,ref}}{d_o}\right) + \frac{RT}{n_{RE}\mathbf{F}}\sum_i^n s_{i,RE}\ln\left(\frac{c_{i,RE}}{d_o}\right) \quad [18]$$

It should be noted that both θ_i and Φ in Eq. [16] and [17] depend on y within the porous layer. In addition, it is assumed that θ_i and Φ are equal to their local bulk solution values within the solution in a pore (*i.e.*, no mass transfer limitations exist within a pore).

Boundary conditions.—To complete the system of equations for the porous electrode region, the boundary conditions must be specified. The porous electrode is bounded by a conductive backing plate (*i.e.*, current collector) on one face ($y = 0$) and by the electrolyte flowing in the channel on the other ($y = S_{PE}$). At both boundaries the electroneutrality condition, Eq. [1], holds. At the backing plate the flux of each species is zero

$$\text{at } y = 0 \qquad N_{ni} = 0 \quad [19]$$

and at the porous electrode/electrolyte interface the flux of each species is continuous

$$\text{at } y = S_{PE} \qquad N_{ni,PE} = N_{ni,E} \quad [20]$$

Expanding Eq. [20] with the flux terms in Eq. [5] and using dimensionless quantities yields

$$\text{at } y = S_{PE}$$

$$\frac{1}{N_{m,PE}}\left(\frac{\partial\theta_i}{\partial\eta}\right)_{PE} + \frac{1}{N_{m,PE}}\frac{z_i\mathbf{F}}{RT}\theta_i\left(\frac{\partial\Phi}{\partial\eta}\right)_{PE} = \left(\frac{\partial\theta_i}{\partial\eta}\right)_E + \frac{z_i\mathbf{F}}{RT}\theta_i\left(\frac{\partial\Phi}{\partial\eta}\right)_E \quad [21]$$

where $\partial\theta_i/\partial\eta$ and $\partial\Phi/\partial\eta$ are determined at the interface but evaluated wholly within the region of their respective subscript.

The dimensionless governing equations and boundary conditions for all regions of the cell are summarized in Table I (2, 14).

Parameters.—The model requires values for fixed parameters of the cell and for the independently adjustable

Table I. Equations describing the Zn/Br_2 cell

I.—Governing equations

a.—Flow channels and separator

$$-\nabla\cdot\mathbf{N}_i + R_i = 0 \quad (i = Br^-, Br_2, Br_3^-) \quad [A]$$

$$\nabla\cdot\mathbf{N}_i = 0 \quad (i = Na^+, Zn^{2+}) \quad [B]$$

$$\Sigma z_i c_i = 0 \quad [1]$$

For the flow channels[a,b]

$$\frac{S^2}{c_{i,ref}D_i}(\nabla\cdot\mathbf{N}_i) \approx -\frac{\partial^2\theta_i}{\partial\eta^2} - \frac{z_i\mathbf{F}}{RT}\left[\theta_i\frac{\partial^2\Phi}{\partial\eta^2} + \frac{\partial\theta_i}{\partial\eta}\frac{\partial\Phi}{\partial\eta}\right] + 3\frac{D_R}{D_i}\mathrm{Pe}\alpha(\eta' - \eta'^2)(\theta_i - 1) \quad [C]$$

and for the separator[a]

$$\frac{S^2}{c_{i,ref}D_{i,e}}(\nabla\cdot\mathbf{N}_i) \approx -\frac{\partial^2\theta_i}{\partial\eta^2} - \frac{z_i\mathbf{F}}{RT}\left[\theta_i\frac{\partial^2\Phi}{\partial\eta^2} + \frac{\partial\theta_i}{\partial\eta}\frac{\partial\Phi}{\partial\eta}\right] \quad [D]$$

where

$$\zeta = x/L \quad [E]$$

$$\eta' = \begin{cases} \dfrac{y}{S_A} & 0 \le y \le S_A \\ \dfrac{y - (S_A + S_S)}{S_A} & (S_A + S_S) \le y \le S \end{cases} \quad [F]$$

$$\mathrm{Pe} = \frac{2Sv_{avg}}{D_R} \quad [G]$$

b.—Porous electrode[a]

Eq. [1], [2], [3], [4]

II.—Boundary conditions

$$\text{at } \zeta = 0 \qquad \theta_i = \theta_{i,feed}; \quad \sum_i z_i c_{i,ref}\theta_{i,feed} = 0 \quad [H]$$

$$\text{at } \eta = 1 \text{ (cathode)} \qquad \frac{s_{i2}\, i_{n2}}{n_2\mathbf{F}} + \frac{s_{i3}\, i_{n3}}{n_3\mathbf{F}} = N_{ni} \quad [I]$$

$$\text{at } y = S_A \text{ (electrolyte/separator)} \qquad N_{ni,E} = N_{ni,S} \quad [J]$$

$$\text{at } y = S_C \text{ (separator/electrolyte)} \qquad N_{ni,S} = N_{ni,E} \quad [K]$$

$$\text{at } y = 0 \text{ (backing/porous electrode)} \qquad N_{ni} = 0 \quad [19]$$

$$\text{at } y = S_{PE} \text{ (porous electrode/electrolyte)} \qquad N_{ni,PE} = N_{ni,E} \quad [20]$$

[a] Simplified by assuming $\alpha << 1$ [see Ref. (13)].
[b] One step model

$$\frac{\partial\theta_i}{\partial\zeta} \approx \frac{\theta_i - 1}{1}$$

parameters. Fixed parameter values used for the Zn/Br_2 cell model here appear in Table II. As in Mader's work (14) the design parameters are set to the Exxon design (5, 15, 16). The reference concentrations, listed in Table II, were chosen based on 50% Zn^{2+} deposition so as to promote their use for both charge and discharge calculations. Note that the reference concentrations and feed concentrations ($c_{i,ref}$ and $c_{i,feed}$) are electrically neutral and that the species Br^-, Br_2, and Br_3^- are in equilibrium according to Eq. [11]. The exchange current densities, $i_{oj,ref}$, and local open-circuit potentials, $U_{j,ref}$, are the values from Ref. (2) and (14) modified to account for the different reference concentrations used here. The relating expressions are

$$U_{j,ref} = (U_{j,ref})_{Mader} + \frac{RT}{n_j\mathbf{F}}\sum_i \ln\left(\frac{(c_{i,ref})_{Mader}}{c_{i,ref}}\right) \quad [22]$$

and

Table II. Fixed parameter values for the Zn/Br_2 cell

Kinetic and thermodynamic (T = 298.15 K)

Reaction (j)	$i_{oj,ref}$[a] (A/cm^2)	α_{aj}	α_{cj}	n_j	U_j^{θ}[b] (V)	$U_{j,ref}$[c] (V)
1	0.001861	0.5	0.5	1	1.087	1.80928
2	0.001861	0.5	0.5	1	1.087	1.80928
3	0.8409	0.5	0.5	1	−0.763	−0.008904

Reaction [4] (Homogeneous, bulk) K_{eq}[d] = 17,000 $(mol/cm^3)^{-1}$.
a, specific surface area of electrode = 25.0 cm^{-1}.

Stoichiometry and electrochemical reaction orders

	Reactions [1] and [2] (j = 1, 2)			Reaction [3] (j = 3)		
Species (i)	s_{ij}	p_{ij}	q_{ij}	s_{ij}	p_{ij}	q_{ij}
Na^+	0	0	0	0	0	0
Br^-[e]	1	1	0	0	0	0
Br_2	−1/2	0	1/2	0	0	0
Zn^{2+}[f]	0	0	0	−1/2	0	1/2
Br_3^-	0	0	0	0	0	0

Transport and reference concentrations

Species (i)	z_i	D_i[g] (cm^2/s) × 10^5	$c_{i,ref}$ (mol/cm^3) × 10^3	$\theta_{i,feed}$[h]
Na^+	1	1.334	1.00	1.000
Br^-	−1	2.084	1.08	2.7306
Br_2	0	1.310	0.05	0.0203
Zn^{2+}	2	0.754	0.50	2.000
Br_3^-	−1	1.310	0.92	0.0554

[a] Chosen to duplicate current densities reported in Ref. (15).
[b] See Ref. (21).
[c] The reference electrode is reaction [3] at Maders' reference conditions.
[d] See Ref. (12).
[e] Limiting reactant at Br_2 electrode.
[f] Limiting reactant at Zn electrode.
[g] See Ref. (18, 22, 23); $D_{Br_3^-}$ assumed equal to D_{Br_2}.
[h] At initial charging conditions, the feed to each channel is assumed to be the same, for convenience. For initial discharge the feed to each channel is the outlet composition after reaching about 60% zinc plated on charge.

$$i_{oj,ref} = (i_{oj,ref})_{Mader} \prod_i \left(\frac{c_{i,ref}}{(c_{i,ref})_{Mader}} \right)^{\gamma_{ij}} \quad [23]$$

where

$$\gamma_{ij} = \begin{cases} p_{ij} - \dfrac{\alpha_{aj} s_{ij}}{n_j} \text{ (anodic)} \\ q_{ij} + \dfrac{\alpha_{cj} s_{ij}}{n_j} \text{ (cathodic)} \end{cases} \quad [24]$$

Equations [22] and [23] follow from Eq. [18] and [16], respectively. Note that in Table II the values for $U_{j,ref}$ are relative to the Zn electrode at Mader and White's (2) reference conditions. In order to confirm the lack of dependence on the choice of the reference electrode the $U_{j,ref}$ were also calculated relative to a hypothetical hydrogen electrode (not shown in Table II) and used in the model. The results using either set of $U_{j,ref}$ were identical.

The input variables to the model include the length of the electrode (L), the average velocity of the electrolyte (v_{avg}), the flow channel width (S_A), the MacMullin number of the separator material (N_m), the thickness of the separator (S_S), the MacMullin number of the porous electrode ($N_{m,PE}$), the thickness of the porous electrode (S_{PE}), the specific active surface area (a) of the porous electrode, and either the applied cell potential ($E_{cell} = V_{PE} - V_c$ on charge and $E_{cell} = V_{PE} - V_a$ on discharge) or the cell current density (i_n). The cell current density is given at the porous electrode/electrolyte interface (*i.e.*, at $y = S_{PE}$) by

$$i_n = \mathbf{F} \sum_i z_i N_i \quad [25]$$

It was determined in Mader's work that only four parameters are independently adjustable in his model: the residence time of electrolyte in the cell (L/v_{avg}), the flow channel width (S_A), the effective separator thickness ($N_m S_S$), and the cell potential (E_{cell}). We found in this work that there exists seven independently adjustable parameters: L/v_{avg}, S_A, $N_m S_S$, the cell potential or current density (E_{cell} or i_n), the porous electrode thickness (S_{PE}), the MacMullin number of the porous electrode ($N_{m,PE}$), and the specific surface area (a).

Here, the effect of the porous electrode on cell performance and the round trip energy efficiency is of major interest. The parameters L, v_{avg}, S_A, S_S, and N_m are held fixed at values used extensively in Mader's work and are values to be expected in a typical Zn/Br_2 flow cell. The specific surface area of the porous electrode material (a) is also held fixed at 25.0 cm^{-1}. Note that a is lumped with the exchange current density in the electrochemical reaction rate expression for the porous electrode (see Eq. [15] and [16]), and it is really their product ($ai_{oj,ref}$) which is held fixed here. The electrode thickness, S_{PE}, is varied from 0.005 to 0.05 cm and $N_{m,PE}$ is varied from 2.0 to 10.0. These ranges seem to encompass values used in industry (17). However, it should be noted that large values of S_{PE}, for example S_{PE} = 0.05 cm, may be too large relative to the flow channel gap, S_A = 0.065 cm, for the assumption of negligible convection in the porous layer to apply.

Implementation of discharge calculations.—The model is used to generate predictions for discharge at constant cell potential and for discharge at constant current density. These two cases are commonly investigated in the literature and represent the two extremes between which discharge occurs in practice. Perhaps discharge at constant external resistance (load) is more appropriate, but this introduces another equation and unknown into the model.

Predictions for discharge at constant cell potential are obtained by changing the cell potential and feed concentration inputs to the model. The cell potential must be set to a value less than the open-circuit potential. The feed concentrations are set to those concentrations existing after reaching a full state-of-charge. Here, the feed concentrations for discharge are the differing exit concentrations in each channel of the cell after reaching about 60% Zn^{2+} plated on charge. For the case with no porous layer, the model by Mader and White (2) could also be used to generate predictions for discharge at constant cell potential given the appropriate inputs.

Predictions for discharge at constant current density are more difficult to obtain. Cell potential (E_{cell}) is not an explicit function of current density (i_n) as evidenced by the Butler-Volmer equation. Hence, an iterative procedure must be used to determine E_{cell} given i_n. Here E_{cell} is treated as an additional unknown, and Eq. [25] is added to the set of equations. The iterative solution procedure used, described next, then solves for E_{cell} along with c_i and Φ.

Method of Solution

The equations describing each region of the Zn/Br_2 cell and the appropriate boundary conditions were solved using Newman's method (18) for the concentration and potential distributions. The one-step model was used here since Mader and White (2) showed that predictions using the two-dimensional model are not significantly different from those of the one-dimensional model for low conversions per pass. The one-dimensional model is appealing because the computation time required is much less than that required for the two-dimensional model (which can be up to 100 times greater). The solution procedure is described by White *et al.* (19) and Mader *et al.* (8). A material balance closure for each species, as given by Mader (14), is done to ensure that the current densities predicted by the model are consistent with the predicted average exit concentrations. Material

balance closure was obtained for all cases presented here.

Results and Discussion

Concentration and potential distributions as functions of state-of-charge are used to analyze the Zn/Br_2 cell model. Performance criteria of interest in the design of this cell have been specified by Mader and White (2) and are used here. First the performance of the cell during charge as a function of the porous electrode parameters is investigated. Second, cell performance during discharge as a function of porous electrode thickness is presented for two cases, one at constant cell potential and the other at constant current density. Third, concentration and potential distributions for charge and discharge are presented and discussed. Lastly, predicted round trip energy efficiencies for charge/discharge cycles of the Zn/Br_2 cell are presented.

Following states-of-charge.—The assumption of a pseudo steady state is used in the model because the concentration and potential distributions in the cell change over relatively long time periods. To follow changes in state-of-charge and cell performance over time, Bellows of Exxon (15) suggests that a convenient parameter to track is the amount of Zn^{2+} which has been consumed and plated on the zinc electrode. The % Zn^{2+} plated is calculated according to Mader and White's (2) definition. Due to the large amount of computer time needed to run consecutive steady-state cases, most studies in the charge mode were limited to 35% Zn^{2+} plated although Bellows (15) reports the system is fully charged when approximately 70% of the Zn^{2+} ions are plated.

In order to propagate the state-of-charge, consecutive steady-state cases are used. That is, the average exit concentrations of the species in both channels for a particular run (state-of-charge) are used as the feed concentrations for the next run. We assume here that the composition exiting the cell at any state-of-charge will eventually be duplicated in the storage tanks and thus in the feed to the anolyte and catholyte channels since the composition of electrolyte is assumed to change slowly under pseudo steady-state conditions. The feed composition of each channel will change independently because the anolyte and catholyte are stored in separate tanks. It should be mentioned that only the feed concentrations ($c_{i,feed}$) are changed to follow state-of-charge. The reference concentrations ($c_{i,ref}$) are held fixed throughout all states-of-charge, and thus the exchange current densities ($i_{oj,ref}$) and reference potentials ($U_{j,ref}$) are fixed at the values reported in Table II. Although the assumptions of pseudo steady-state operation and that the exit composition at one state-of-charge is the feed composition to a future state-of-charge are valid only for low conversion per pass, these assumptions at least provide a rough estimate of cell performance as a function of state-of-charge. A time-dependent model could be prepared to determine the validity of this pseudo steady-state assumption.

Model predictions at various states-of-charge.—Figures 2 and 3 show the effect of porous electrode parameters on total cell energy efficiency (ϵ_T) during charge. The cases studied for the charge mode include three porous electrode thicknesses and three MacMullin numbers for the porous electrode. The parameters L/v_{avg}, S_A, and N_mS_S are held fixed in this work since only the effects of porous electrode parameters are of primary interest. The residence time of the electrolyte in the cell (L/v_{avg}) is 15s, the flow channel width (S_A) is 0.065 cm, and the effective separator thickness (N_mS_S) is 0.18 cm. These values are used extensively in Mader's work (14) and are values to be expected in a typical Zn/Br_2 flow battery. The cell potential, E_{cell}, is held fixed at 1.9V to parallel Mader's work (14).

Figure 2 illustrates the predicted effect of the thickness of the porous electrode (S_{PE}) on total cell energy efficiency (ϵ_T) during charge. The curves in Fig. 2 slope upward, reach a maximum, then slope downward. This shape is seen in similar plots in Mader and White's work (2) and is attributed to the changing reactant concentrations as the state-of-charge changes. Note that as S_{PE} is increased the efficiency increases as well. This result was expected because the greater the thickness of the electrode the greater amount of surface area is available for electrochemical reaction when conditions are kinetically controlled as is the case here. This finding that the electrochemical reaction rate is limited by the electrode kinetics rather than by the transport of species to the reactive surfaces is discussed later. The thickness used for the porous electrode in the model must be limited because as S_{PE} approaches S_A, convection through the porous electrode and hence pressure differentials would become important and the assumption that these contributions to transport are negligible would be invalid. Figure 2 demonstrates a much improved predicted efficiency when using a porous electrode as opposed to a flat plate electrode used in earlier work (2). Comparing Fig. 2 with Fig. 6 of Mader and White (2) an improvement in efficiency of at least 10% is realized at any given state-of-charge. Also note that the maximum efficiency is reached at a later state-of-charge with the porous electrode. This shift of the maximum toward the midpoint of the charge/discharge cycle may be considered as an improvement in the efficiency distribution during charge.

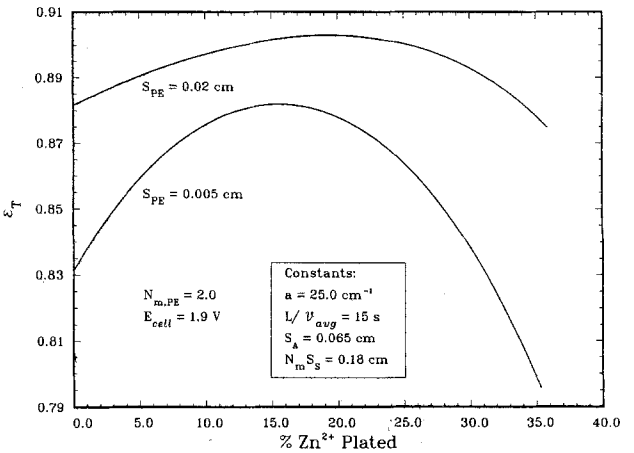

Fig. 2. Effect of porous electrode thickness (S_{PE}) on cell efficiency during charge.

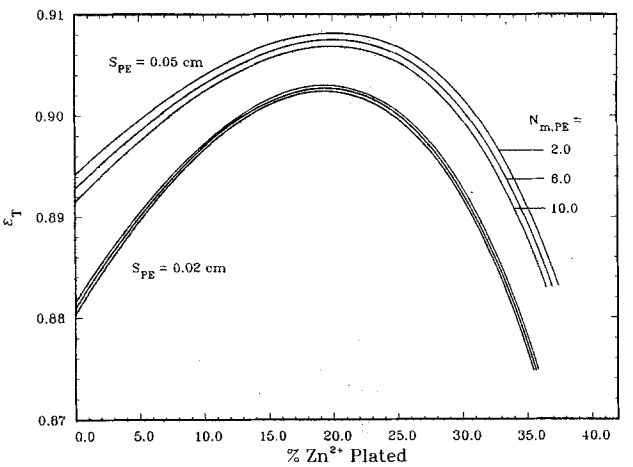

Fig. 3. Effect of porous electrode MacMullin number ($N_{m,PE}$) on cell efficiency during charge.

Figure 3 shows the predicted effect of $N_{m,PE}$ on cell efficiency. The shapes of the curves are similar to those in Fig. 2 and for the same reasons. $N_{m,PE}$ exhibits relatively little effect on efficiency even at a relatively large value of S_{PE} where its effect becomes more pronounced. As will be discussed later, concentration gradients within the porous electrode are small. Diffusion and migration of species into the porous electrode play a minor role in the cell operation under the conditions considered here and hence the effective diffusivity ($D_i/N_{m,PE}$) and thus the MacMullin number does not have a significant effect on

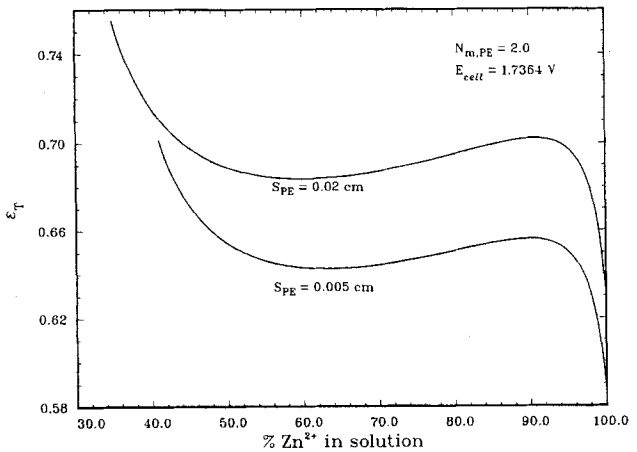

Fig. 4. Cell efficiency during discharge at constant cell potential

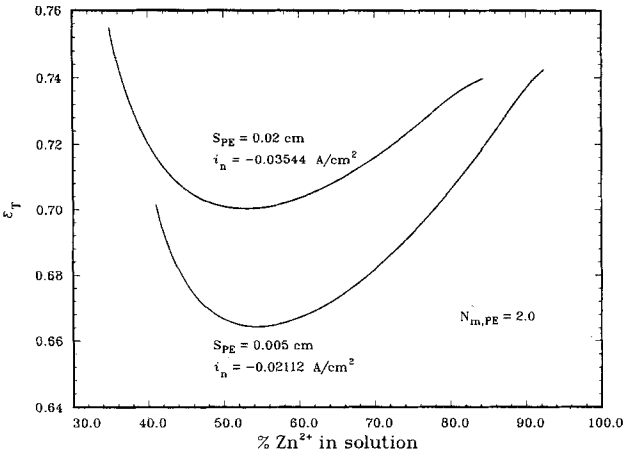

Fig. 6. Cell efficiency during discharge at constant current density

the predictions. Consequently, $N_{m,PE}$ will be held fixed at a value of 2.0 for the remainder of this work.

Model predictions at various states-of-discharge.—Cell performance is investigated here for discharge at constant cell potential and discharge at constant current density. Note that only the charge mode at constant cell potential was considered in the previous section even though the model could be used to generate predictions for a constant current density charge. For discharge, changes in the state-of-charge are followed by tracking the percent Zn^{2+} ions in solution (= 100%-% Zn^{2+} plated).

Consider first discharge at constant cell potential. Figure 4 is analogous to Fig. 2 and presents cell efficiency as a function of the state-of-charge. The curves reach maxima and minima due to the changing electrolyte compositions as the state-of-charge changes and due to the competing electrochemical reactions at the zinc electrode. Also, lower efficiencies are obtained for thinner porous electrodes, as is expected. Figure 5 illustrates how the current density changes throughout the discharge. The current density decreases as the cell is discharged due to depletion of reactants. Note that the model predicts this decrease to be almost linear.

Consider next discharge at constant current density. Figure 6, analogous to Fig. 2 and 4, shows that efficiency decreases as the porous electrode thickness is decreased. Again, the shape of the curves is attributed to the changing concentrations and competing reactions at the zinc electrode. Figure 7 illustrates the drop in cell potential during discharge at constant current density. The model predicts the cell potential to drop almost linearly for some time until approaching full discharge at which point the cell potential drops off dramatically. This ending behavior is due to the depletion of bromine in the porous electrode which gives rise to a concentration overpotential thus decreasing the cell potential.

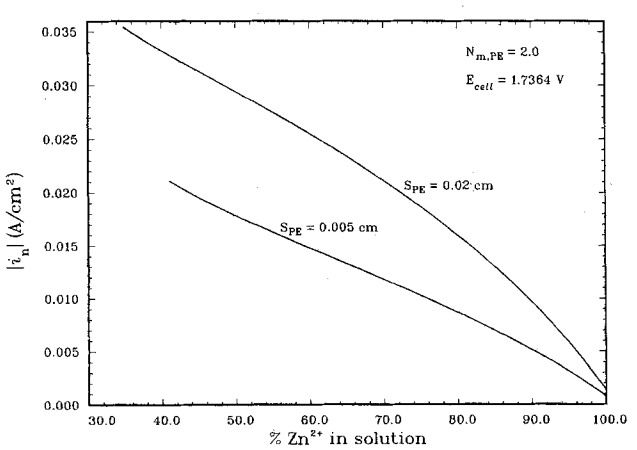

Fig. 5. Current density during discharge at constant cell potential

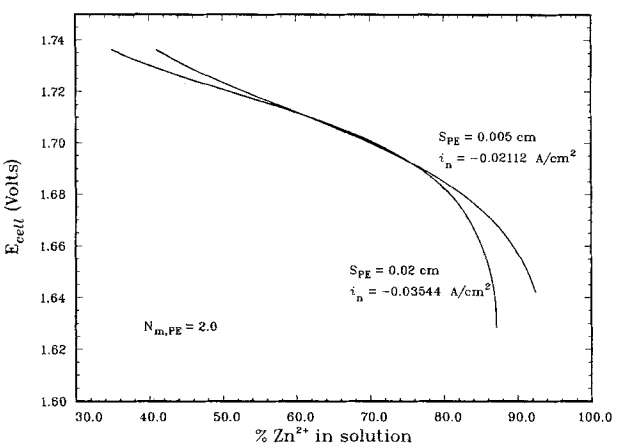

Fig. 7. Cell potential during discharge at constant current density

The reader is cautioned not to compare the constant cell potential and constant current density discharge cases. These are two separate cases, commonly studied because of ease and because they represent two extreme cases, with no common basis for comparison. As mentioned earlier, discharge at constant external load is perhaps more appropriate to consider. It should be mentioned that the initial current densities from the runs at constant cell potential were used as the current densities for the runs at constant current density. Note that the curves for each S_{PE} value in Fig. 6 begin at the same efficiencies as the two curves in Fig. 4.

In addition, it is worth noting that some researchers have suggested that the corrosion of zinc by bromine

$$Zn(s) + Br_2(aq) \rightarrow Zn^{2+}(aq) + 2Br^-(aq) \quad [26]$$

occurs at the zinc electrode and that this reaction is independent of potential. This reaction does not take place during charge because the zinc is cathodically protected; the bromine reduction reaction depends on potential and competes with the zinc deposition reaction as illustrated in Fig. 1. During discharge, the bromine reaction is a reduction reaction, whereas zinc is oxidized, and the rates of both reactions depend upon potential.

Concentration and potential profiles.—Concentration and potential profiles for both charge and discharge modes of the Zn/Br_2 cell are shown in Fig. 8-10. These profiles are those predicted at a state-of-charge of about 35% Zn^{2+} plated which is approximately the halfway mark between the initial charge and discharge conditions used here.

Note in Fig. 8 and 9 the portions of the concentration profiles within the porous electrode region. These portions are almost straight horizontal lines indicating no significant resistance to diffusion and migration of species into and out of the porous electrode. Thus, within the porous electrode the reaction rate is kineti-

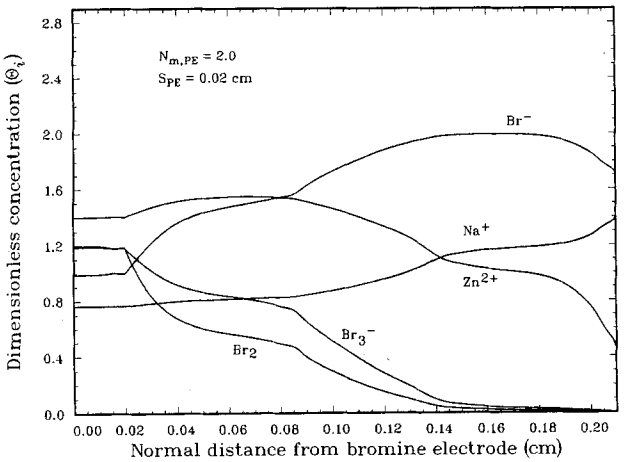

Fig. 8. Concentration profiles in the radial direction during charge at a state-of-charge of 35% Zn^{2+} plated.

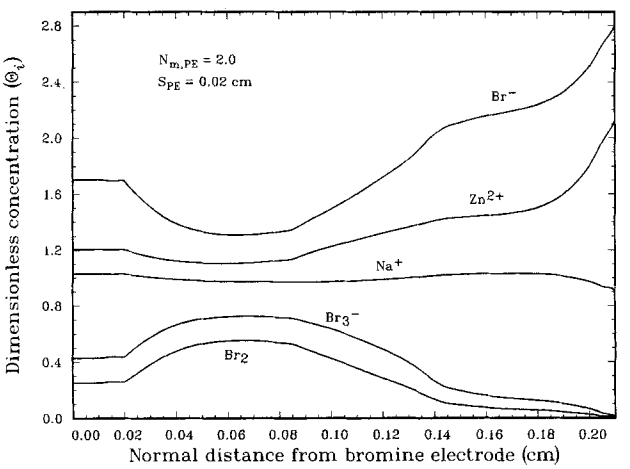

Fig. 9. Concentration profiles in the radial direction during discharge at constant current density at a state-of-charge of 35% Zn^{2+} plated.

cally controlled rather than diffusion controlled. Under these conditions the optimal thickness of the porous electrode is the thickest possible. Since the reaction rate is kinetically controlled a thicker porous electrode offers greater surface area hence more reaction. The greater amount of reaction at the porous bromine electrode requires a greater amount of reaction at the zinc electrode. The zinc reaction accommodates this increase to a greater extent than does the parasitic bromine reaction (because the exchange current density for the zinc reaction is several orders of magnitude larger than that for the bromine reaction), and hence an increase in coulombic efficiency is realized. These results were shown earlier in Fig. 2. However, a trade off exists between increasing coulombic efficiency and decreasing voltaic efficiency as the porous electrode thickness is increased. As the porous electrode thickness is increased the volume of electrolyte in the pores increases, hence there is an increase in resistance to current flow and a corresponding decrease in voltaic efficiency.

The transport controlled problem in the porous electrode may be investigated by changing the kinetic parameters or the specific surface area (a). The kinetic parameter values used here, listed in Table II, are those obtained from Mader's work (14). These values were determined by trial and error so as to give predictions comparable to experimental data reported in the literature. Note that these exchange current densities are an order of magnitude smaller than those reported earlier (20). Small exchange current densities lead to small electrochemical reaction rates and hence a kinetically controlled reaction rate. Changing the kinetic parameters or the specific surface area so as to obtain a transport limited design and still obtain predictions comparable to

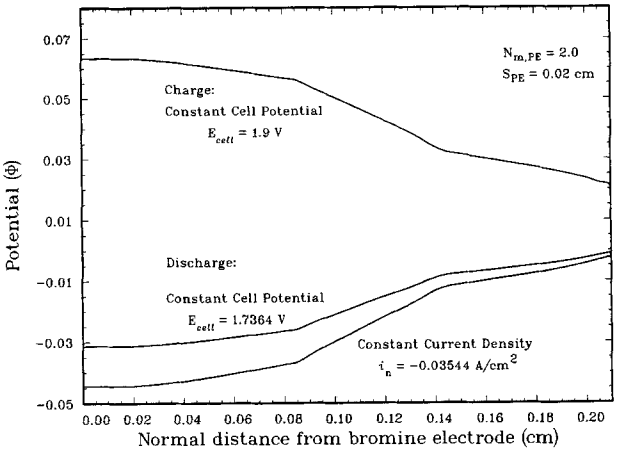

Fig. 10. Ohmic drop in cell at a state-of-charge of 35% Zn^{2+} plated

experimental values reported in the literature is beyond the scope of this work.

The remaining portions of the concentration profiles in Fig. 8 and 9 exhibit several features. First, the concentration gradients are seen to be rather large in the flow channels. This result indicates that the assumption of constant electrolyte composition in the flow channels used in some models (3-5) may be inappropriate. Also, the profiles are fairly linear in the separator region. Such linear profiles are often assumed to be valid and used in the separator regions of cell models. Finally, the reaction rate at the zinc electrode appears to be transport limited on charge as evidenced by the rather steep concentration gradient for Zn^{2+} in the vicinity of the electrode surface in Fig. 8.

In Fig. 10 the potential profiles for charge and discharge are seen to mirror each other, as expected. The IR-drop in the cell for a given state-of-charge and mode of operation is equal to the drop in Φ from the current collector/porous electrode interface to the flat plate zinc electrode.

Round trip energy efficiency.—An effective measure of battery performance is its round trip energy efficiency (*RTEE*). This quantity is simply the ratio of energy drained from the battery (discharge mode) to energy input to the battery (charge mode) for a given cycle on a percentage basis. *RTEE* is obtained from the model predictions here using the following equation

$$RTEE = \frac{\int_{s_2}^{s_1} (IE_{cell})_{discharge}\, ds}{\int_{s_1}^{s_2} (IE_{cell})_{charge}\, ds} \times 100\% \qquad [27]$$

The symbols s_1 and s_2 represent different states-of-charge (% Zn^{2+} plated). The product IE_{cell} is a power term (energy per unit time) and changes as the state-of-charge changes. It is assumed in writing Eq. [27] that the residence time for charge is equal to the residence time for discharge so that the result is a ratio of energies. This assumption seems reasonable and at least provides an estimate of *RTEE*.

Round trip energy efficiencies for four cases investigated here are shown in Table III. These values were calculated by arbitrarily choosing a window in the charge/

Table III. Round trip energy efficiencies

Values listed are round trip energy efficiencies for constant E_{cell} charge and either constant E_{cell} or constant i_n discharge

	Constant E_{cell} discharge (%)	Constant i_n discharge (%)
S_{PE} = 0.02 cm	41.86	69.16
S_{PE} = 0.005 cm	36.46	64.44

discharge cycle of 20-40% Zn^{2+} plated. It seems reasonable to assume that a midrange portion of the entire charge/discharge cycle should be indicative of the entire cycle when estimating cycle quantities. Note that higher *RTEE*'s are obtained for the thicker porous electrode indicating that the optimal porous electrode thickness would be the thickest possible. The thickness of the porous electrode is limited due to decreasing voltaic efficiency and because the assumption of negligible transport due to convection in the porous electrode becomes invalid as discussed earlier. Also, for the arbitrarily chosen values of i_n and E_{cell} used here, the results for discharge at constant current density yield higher efficiencies than those for discharge at constant cell potential. Higher efficiencies are obtained for the constant current density case because the unwanted bromine reduction reaction at the zinc electrode is less important in this case than it is for constant cell potential discharge. However, it is difficult to compare these two cases, as discussed earlier, but they do provide a feel for the *RTEE*'s which are possible. Perhaps by choosing a different value for E_{cell} (further away from the open-circuit potential), the results for discharge at constant cell potential would compare more favorably with those obtained for the constant current density discharge. Based on the results in Table III a *RTEE* of 70% should be attainable.

Conclusions

The Zn/Br_2 cell model presented here could be a useful tool for the design of the Zn/Br_2 flow battery and could save time, money, and effort if used in place of building and testing many different designs. The model is used to show that an optimal porous electrode thickness should exist for a given set of design criteria. For the kinetically controlled reaction rate in the porous bromine electrode here the largest electrode thickness of those studied was the optimum thickness. The model can predict both charge and discharge conditions and provides an estimate of the round trip energy efficiency (*RTEE*). The predictions suggest that a *RTEE* of 70% or more should be possible. The model could be extended to include additional complexities such as a second bromine-rich phase sometimes called the "red oil" phase.

Manuscript received June 13, 1986; revised manuscript received Oct. 17, 1986.

LIST OF SYMBOLS

a	specific electroactive surface area of the porous electrode, cm^{-1}
c_i	concentration of species i, mol/cm^3
$c_{i,feed}$	feed concentration of species i, mol/cm^3
$c_{i,ref}$	reference concentration of species i, mol/cm^3
D_i	diffusion coefficient of species i, cm^2/s
$D_{i,e}$	effective diffusion coefficient of species i in the separator, cm^2/s
$D_{i,e,PE}$	effective diffusion coefficient of species i in the porous electrode, cm^2/s
d_o	density of pure solvent, kg/cm^3
D_R	diffusion coefficient of limiting reactant, cm^2/s
E_{cell}	applied cell potential ($=V_a - V_c$), V
F	Faraday's constant, 96,487 C/mol
I	total cell current, A
i_n	total current density at an electrode ($=I/LW$), A/cm^2
$i_{oj,ref}$	exchange current density of electrochemical reaction j, A/cm^2
j_j	current density due to electrochemical reaction j, A/cm^2
K_{eq}	equilibrium constant for tri-bromide reaction, cm^3/mol
L	electrode length, cm
L/v_{avg}	residence time of the reactor, s
$\mathbf{N}_i$	flux vector of species i, mol/cm^2-s
n_j	number of electrons passed in reaction j
N_m	MacMullin number in the separator
$N_{m,PE}$	MacMullin number in the porous electrode
$N_m S_S$	effective separator thickness, cm
N_{ni}	normal component of the flux (y- or η-direction) of species i, mol/cm^2-s
$N_{ni,E}$	normal component of the flux of species i in the electrolyte, mol/cm^2-s
$N_{ni,PE}$	normal component of the flux of species i in the porous electrode, mol/cm^2-s
$N_{ni,S}$	normal component of the flux of species i in the separator, mol/cm^2-s
p_{ij}	anodic reaction order of species i in reaction j
Pe	Peclet number ($=2Sv_{avg}/D_R$)
q_{ij}	cathodic reaction order of species i in reaction j
R	gas law constant, 8.314 J/mol-K
R_i	homogeneous reaction rate, mol/cm^3-s
R'_i	electrochemical reaction rate, mol/cm^3-s
RTEE	round trip energy efficiency
s	state-of-charge (% Zn^{2+} plated)
s_1	state-of-charge 1
s_2	state-of-charge 2
s_{ij}	stoichiometric coefficient of species i in reaction j
S	total electrode gap, cm
S_A	anolyte channel width, cm
S_C	catholyte channel width, cm
S_{PE}	thickness of the porous electrode, cm
S_S	thickness of the separator, cm
T	temperature, K
U_j^θ	standard half-cell potential, V
$U_{j,ref}$	open-circuit potential of reaction j based on the reference concentrations, V
V_a	anode potential, V
v_{avg}	average velocity of the electrolyte, cm/s
V_c	cathode potential, V
V_{PE}	potential of porous electrode, V
W	width of the electrode, cm
x	axial coordinate, cm
y	normal coordinate, cm
z_i	charge number of species i

Greek

α	aspect ratio, S/L
α_{aj}	anodic transfer coefficient for reaction j
α_{cj}	cathodic transfer coefficient for reaction j
ϵ	porosity of porous electrode material
ϵ_C	coulombic efficiency
ϵ_T	total cell energy efficiency
ϵ_V	voltaic efficiency
ζ	dimensionless axial coordinate (x/L)
η	dimensionless normal coordinate (y/S)
η_j	overpotential at electrode surface ($V_e - \Phi_{oe} - U_{j,ref}$), V
η'	dimensionless normal coordinate, specific to a flow channel
θ_i	dimensionless concentration of species i ($c_i/c_{i,ref}$)
$\theta_{i,feed}$	dimensionless feed concentration of species i
τ	tortuosity of porous electrode material
Φ	solution potential, V

Subscripts

A	anolyte
a	anode
C	catholyte
c	cathode
E	electrolyte
i	species i
j	reaction j
n	normal component
PE	porous electrode
RE	reference electrode
S	separator

REFERENCES

1. J. L. Chamberlin, in "Proceedings of the EPRI/LBL Workshop on the Electrochemistry of Zinc/Halogen Batteries," Vol. 1, p. 2, Palo Alto, CA, Nov.30-Dec. 1, 1983 (1984).
2. M. J. Mader and R. E. White, *This Journal*, **133**, 1297 (1986).
3. J. Lee and J. R. Selman, *ibid.*, **129**, 1670 (1982).
4. J. Lee, Ph.D. Thesis, Illinois Institute of Technology, Chicago, IL (1981).
5. J. W. Van Zee, R. E. White, P. Grimes, and R. Bellows, in "Electrochemical Cell Design," R. E. White, Editor, p. 293, Plenum Publishing Co., New York (1984).
6. P. S. Fedkiw and R. W. Watts, *This Journal*, **131**, 701 (1984).
7. L. H. Thaller, NASA TM X-71540 (1974).
8. M. J. Mader, C. W. Walton, and R. E. White, *This Journal*, **133**, 1124 (1986).

9. D. L. Caldwell, K. A. Poush, J. W. Van Zee, and R. E. White, in "Electrochemical Process and Plant Design," R. C. Alkire, T. R. Beck, and R. D. Varjian, Editors, p. 216, The Electrochemical Society Softbound Proceedings Series, Pennington, NJ (1983).
10. K. A. Poush, D. L. Caldwell, J. W. Van Zee, and R. E. White, in "Modern Chlor-Alkali Technology," Vol. II, C. Jackson, Editor, p. 21, Ellis Horwood Limited, Chichester, West Sussex, England (1983).
11. J. W. Van Zee, Ph.D. Thesis, Texas A&M University, College Station, TX (1984).
12. M. Eigen and K. Kustin, *J. Am. Chem. Soc.*, **84,** 1355 (1962).
13. T. V. Nguyen, C. W. Walton, R. E. White, and J. W. Van Zee, *This Journal*, **133,** 81 (1986).
14. M. J. Mader, M. S. Thesis, Texas A&M University, College Station, TX (1985).
15. R. Bellows, in "Proceedings of the EPRI/LBL Workshop on the Electrochemistry of Zinc/Halogen Batteries," Vol. I, p. 4, Palo Alto, CA, Nov. 30-Dec. 1, 1983 (1984).
16. R. Bellows, P. Grimes, H. Einstein, E. Kantner, P. Malachesky, and K. Newby, *IEEE Trans. on Veh. Tech.*, **VT-32,** 26 (1983).
17. P. Grimes, Personal communication, August 1985.
18. J. S. Newman, "Electrochemical Systems," Prentice-Hall, Inc., Englewood Cliffs, NJ (1973).
19. R. E. White, M. Bain, and M. Raible, *This Journal*, **130,** 1037 (1983).
20. J. W. Van Zee and R. E. White, *ibid.*, **130,** 2003 (1983).
21. "CRC Handbook of Chemistry and Physics," 60th ed., CRC Press, Inc., Boca Raton, FL (1979).
22. R. E. White, in "Proceedings of the EPRI/LBL Workshop on the Electrochemistry of Zinc/Halogen Batteries," Vol. I, p. 5, Palo Alto, CA, Nov.30-Dec. 1, 1983 (1984).
23. R. Selman, in "Proceedings of the EPRI/LBL Workshop on the Electrochemistry of Zinc/Halogen Batteries," Vol. II, p. 10, Palo Alto, CA, Nov. 30-Dec. 1, 1983 (1984).

The Influence of Organic Solvents on Aromatic Adsorption at Platinum

Acetic Acid, Acetone, Acetonitrile, Dimethylacetamide, Dimethylsulfoxide, Sulfolane, and Tetrahydrofuran

Dian Song, Manuel P. Soriaga,[1] and Arthur T. Hubbard[2]

Department of Chemistry, University of California, Santa Barbara, California 93106

ABSTRACT

The influence of nonaqueous solvents on the packing density and electrochemical reactivity of 2,2',5,5',-tetrahydroxybiphenyl (THBP) chemisorbed at smooth polycrystalline Pt electrodes has been studied using thin layer electrochemical techniques. THBP was chosen as the model polyphenolic compound because its surface coverage is readily measured, and it displays electrochemical reactivity in the adsorbed state which is a function of its orientation. The nonaqueous solvents employed were: acetonitrile, ethyl acetate, acetone, acetic acid, dimethylacetamide, tetrahydrofuran, dimethylsulfoxide, and sulfolane. Adsorption of THBP from its aqueous solutions led to three different orientation states (flat, edge-edge, and edge-pendant) which depended upon the THBP concentration. The edge-pendant state showed reversible quinone/diphenol reactivity similar to that in the unadsorbed state. Changes in the adsorption behavior and electrochemical reactivity of THBP was noted when 10 m*M* of organic solvent was added. The extent of change depended upon the adsorbability of the added solvent, being least noticeable with ethyl acetate (which is not chemisorbed on Pt) and most dramatic with dimethylsulfoxide (which is very strongly chemisorbed on Pt). The more strongly adsorbing of these solvents virtually eliminated adsorption of THBP in the flat orientation. The electrochemical reactivity of THBP adsorbed in the edge-pendant orientation was sensitive to the nature of the nonaqueous solvent, probably because of solvent adsorbate interactions. These results provide revealing glimpses of the role played by oriented adsorbed intermediates and nonaqueous solvents in the stereospecificity of organic electrochemical reactions. In particular, the data appear to invalidate previous assumptions that the orientation of adsorbed aromatic intermediates is flat, regardless of solute concentration or nature of the solvent.

Systematic studies (1-5) with atomically smooth polycrystalline Pt thin layer electrodes have demonstrated that a wide variety of organic reagents are spontaneously and irreversibly adsorbed from aqueous solutions onto the electrode surface to form a stable monolayer consisting of close-packed molecules attached in specific, identifiable orientations. For example, chemisorption of single aromatics at low concentrations ($\leq$0.1 m*M*) from aqueous solutions not containing other adsorbates led to flat oriented intermediates, while adsorption of the same compounds at higher concentrations ($\geq$1 m*M*) yielded vertically oriented species; these adsorbed molecule orientations have been verified by reflection-adsorption infrared spectroscopy. It has also been found that orientational phase transitions within the organic layer can be triggered by changes in solute (adsorbate) concentration, pH, temperature, and coadsorption of other surface active species; flat-to-vertical orientational transitions displayed by aromatic and quinonoid compounds are suppressed at roughened surfaces. Adsorbed molecule orientation has been shown to exert a strong influence on the surface chemistry of the adsorbate itself and on the electrochemical reactivity of unadsorbed redox couples (1-5). In particular, the extent of irreversible oxidation or hydrogenation was much greater for intermediates adsorbed in flat than in vertical orientations.

It is important to extend the above studies to include the influences of nonaqueous solvents since, in numerous organic electrochemical reactions, the product distributions are often characterized by features not readily understood in terms of concepts derived from homogeneous solution chemistry (6). In such cases, the heterogeneity of the electrode reaction is often invoked, and the electrode surface is thought to exert steric influence on chemical reactions which occur following electron transfer. Concepts such as "steric shielding by the electrode from attack on one side of the substrate/intermediate" (6) are not uncommon, and have been offered to account for the stereochemistry of electrode processes. The participation of the electrode in this manner, of course, implies the existence of reaction intermediates adsorbed in stable orientational states. That is, adsorbed molecule orientation plays an important role in many organic electrochemical reactions (7).

It is expected that the results obtained in aqueous solutions will differ from those in nonaqueous solvents

[2]Present address: Department of Chemistry, University of Cincinnati, Cincinnati, Ohio 45221.